Sputtering of high-energy particles from the Ag{100} surface

Che-Chen Chang* and Jiin-Yun Hsieh
Department of Chemistry, National Taiwan University, Taipei, Taiwan, Republic of China
(Received 8 September 1997; revised manuscript received 29 January 1998)

The sputtering of atoms with high kinetic energies of hundreds of eV from the single-crystal surface due to energetic particle bombardment is studied using Ag{100} as a model system. Molecular-dynamics calculations show that these high-energy atoms tend to be preferentially sputtered along a major crystallographic direction, along which the atoms with sputtering energies of less than 50 eV are known to exhibit the minimum sputter intensity. The angular anisotropy exhibited in the azimuthal angle distribution of the high-energy atoms is mainly due to the anisotropic sputtering of the atoms from the second layer. Collision cascade analysis shows that the high-energy atoms may be ejected from the surface by a collision either directly from the primary particle or from a fast-moving surface particle after it travels energetically in a space between two adjacent {100} atomic planes perpendicular to the surface. At high ejection energies, there is also a significant increase in the relative contribution of the atoms sputtered from below the first atomic layer to the total sputter yield. The high-energy atoms ejecting from the lower layers tend to be focused to pass through the center of a triangular atomic feature on the surface, and then confined by a surface semichannel before leaving the surface. The use of the high-energy atoms for surface structural determination is discussed. The angular distribution of the low-energy atoms reflects more of the geometric structure of the first atomic layer, whereas the high-energy atoms exhibit more of the structural property of the second layer. [S0163-1829(98)05019-X]

I. INTRODUCTION

During the last two decades, there has been considerable interest in developing surface-sensitive techniques for determining chemical bonding geometry on surfaces.[1] In particular, angle-resolved secondary particle mass spectrometry has emerged as a valuable tool for surface structural analysis due to its high sensitivity to various masses in the top layers of a solid.[2–10] Most angle-resolved secondary particle mass spectrometric studies performed so far were focused on the properties of the particles sputtered from the surface with kinetic energies of less than 50 eV. When sputtered from the single-crystal surface, these particles exhibit preferred azimuths of sputtering which are along open crystallographic directions of the surface. The preferred azimuth of sputtering thus varies with the face of the crystal exposed,[11–14] as well as with the registry and the height of the adsorbate.[6(b),15–17] By examining the angular distribution of the sputtered particles, the original atomic arrangement of the crystal surface may be determined.

The present study is aimed at understanding the sputtering behavior of high-energy atoms from the surface, and exploring the possibilities of utilizing these atoms for surface analysis. The high-energy range with which this study is concerned is in the regime of more than 150 eV. It was known from energy- and angle-resolved studies[4] of sputtered particles that the angular distribution of these particles might change with the kinetic energy of these particles.[7,9,17–19] Other previous studies showed that although the preferred azimuth of sputtering might change with the polar angle of detection,[5] it did not vary with the ejection energy of the sputtered particles. There have been very few studies[20] focused on the relationship between the kinetic energy of the sputtered particles and the peak position, which reflects to some extent the geometric structure of the surface, in the azimuthal angle distribution of these particles. Furthermore, details of the sputtering process of the particles with high ejection energies of more than 150 eV are also very much unknown. These particles eject from the surface very early in the collision cascade, when the surface structure is quite intact. The present study investigates the fundamental collision processes that result in sputtering of the high-energy particles in order to see (a) if some structural features on the surface are able to constrain these high-energy particles to eject along specific crystallographic directions; (b) whether and how the peak azimuth in the angular distribution is influenced, as the kinetic energy of sputtering is increased by the detail of the collision process; and (c) if additional structural information about the surface may be obtained from the sputtering of the high-energy particles. We find that by detecting both low- and high-energy particles sputtered from the surface, more complete information about the surface properties may be obtained.

II. DESCRIPTION OF THE CALCULATION

A molecular-dynamics procedure[21–24] is employed for this work to compute the dynamics of the atom-surface collision process. The procedure utilizes a microcrystallite of more than 1200 Ag atoms with ~ 1000 Å^2 in size per layer. The primary particles of Ar atoms are allowed to impinge normal to the Ag{100} surface in the static mode, and to interact simultaneously, via a sum of pairwise additive potentials, with all of the substrate atoms. Time-dependent positions and momenta of all the particles are then calculated by numerically integrating Hamilton's equations of motion.

The nature of the interaction between the primary particle and the surface atoms is assumed to be a Moliere type,[25] with the Thomas-Fermi screening length adjusted according to the Firsov model[26] and the formula of Ref. 27. In addition, since

high-energy events are the main concern of the present study, the pairwise potential is employed for computational ease to describe the interaction among the surface atoms. At large interatomic distances, these atoms interact with each other according to pairwise additive forces derived from the Morse potential. The depth of the attraction well is at 0.417 eV. At small distances, the interaction of the surface atoms is described by the Moliere potential. The two interaction potentials are fitted by a cubic spline at about half the distance from the nearest neighbors on the surface. The interaction vanishes smoothly at a distance greater than the one corresponding to the separation from the second-nearest neighbors. The results of the calculation based on these interaction potentials agree well with the experimental measurements.[28]

To obtain sufficient sampling statistics on high-energy sputtering events, exponentially increasing sets of Ar impacts (i.e., 200, 400, 800, 1600,. . .), which are distributed uniformly within the irreducible zone of symmetry[29] on the surface, are calculated. Statistical convergence is assessed by examining the angular distributions of the atoms sputtered with kinetic energies of more than 150 eV from different atomic layers. The calculations are terminated when the kinetic energy of each atom in the system is less than 100 eV. Comparisons of the layer-resolved angular distributions between consecutive sets of Ar impacts show that similar angular distributions are not present until a set of 12 800 trajectories are calculated. Results from the calculation of the 12 800 trajectories are then used for the ejection mechanistic study and the quantitative analysis of the atoms sputtered with kinetic energies of more than 150 eV from the surface. To extract information about the sputtering of the atoms from the surface with kinetic energies of less than 50 eV, a separate set of 3200 Ar impacts are calculated. The collision cascades initiated by the incidences of these 3200 Ar atoms are terminated when the kinetic energy of each atom in the system is less than 0.2 eV. The polar angle of ejection used in constructing angular distributions is defined from the surface normal. The distributions are presented after a moving-window boxcar average of the data.

III. RESULTS AND DISCUSSION

The dependence of the angular distribution of sputtered particles on the kinetic energy of ejection is studied to see if the high-energy particles have distributions similar to those of the low-energy particles. In previous studies,[7,9,17–19] the azimuth along which the maximum sputter intensity occurred was found to be independent of the kinetic energy of sputtered particles in the low-energy regime of less than 50 eV. For particles sputtered from a clean surface, the maximum intensity usually occurs along an open channel, such as along the ⟨211⟩ azimuth of a fcc{111} surface or the ⟨100⟩ azimuth of a fcc{100} surface, along which emitting atoms are least obstructed. Results from a recent sputtering study,[16] however, showed that, for high-energy atoms sputtered from the Ag{111} surface, the peak position in the azimuthal angle distribution may be sensitive to variations in the ejection energy. The sensitivity was due to the fact that there were two different groups of the ⟨211⟩ azimuth on the fcc{111} surface. The atom may be sputtered preferentially along either of the two ⟨211⟩ directions. One might thus predict that for the case of atoms sputtered from the fcc{100} surface, the peak angle in the azimuthal angle distribution should not vary with the ejection energy, since there is only one group of the ⟨100⟩ azimuth on the surface along which emitting atoms are least obstructed.

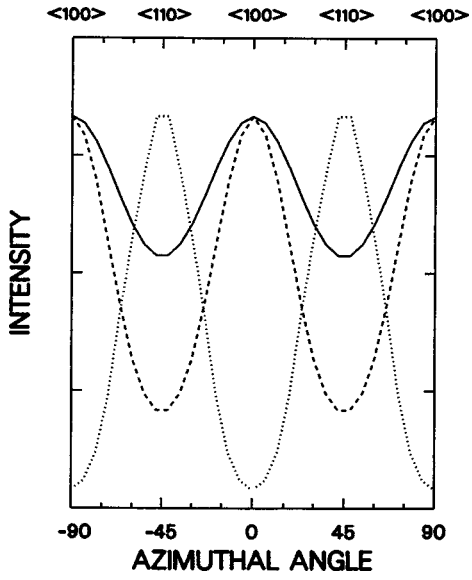

FIG. 1. Calculated dependence on azimuthal angle of Ag atoms sputtered with various ejection energies for a clean Ag{100} surface bombarded by 2-keV Ar atoms at normal incidence. The polar angle of detection is 45°, and the angular resolution is ±7°. The solid curve represents the normalized dependence for atoms ejecting with kinetic energies between 0.4 and 2 eV, the dashed curve the one between 20 and 40 eV, and the dotted curve the one between 220 and 240 eV. Both the solid and dashed curves are constructed from calculation results of 3200 incidences, and the dotted curve from results of 12 800 incidences.

Plotted in Fig. 1 are examples of three azimuthal angle distributions obtained at a polar angle of 45° for atoms sputtered from a Ag{100} surface with kinetic energies of 1.2 ±0.8, 30±10, and 230±10 eV, respectively. As shown in the figure, atoms sputtered with kinetic energies of 1.2±0.8 and 30±10 eV ''prefer'' to proceed along the ⟨100⟩ direction. The peak position in the spectra is not sensitive to the ejection energy in these low-energy ranges, in agreement with the prediction and with the results of previous studies on Rh{100}.[7,18,19] Further increasing the detection energy of the sputtered particles, however, has a significant effect on the azimuthal angle distribution. The azimuth at which the maximum sputter intensity is observed shifts as the ejection energy is increased from 30±10 to 230±10 eV. In fact, the preferred direction of sputtering changes from one low-index crystallographic direction to another. The sputter intensity at the ⟨100⟩ azimuth decreases from its maximum to its minimum, and the peak position shifts from the ⟨100⟩ azimuth to the ⟨110⟩ azimuth as the ejection energy is increased.

To understand why the high-energy atoms are more sputtered along the ⟨110⟩ azimuth, rather than along the less obstructed ⟨100⟩ direction, the spot pattern[11] of the sputtered atoms from different atomic layers of the surface is then studied. Figures 2(a)–2(d) show the spot pattern of the Ag atoms sputtered from either the first or second atomic layer with kinetic energies of 30±10 and 230±10 eV, respec-

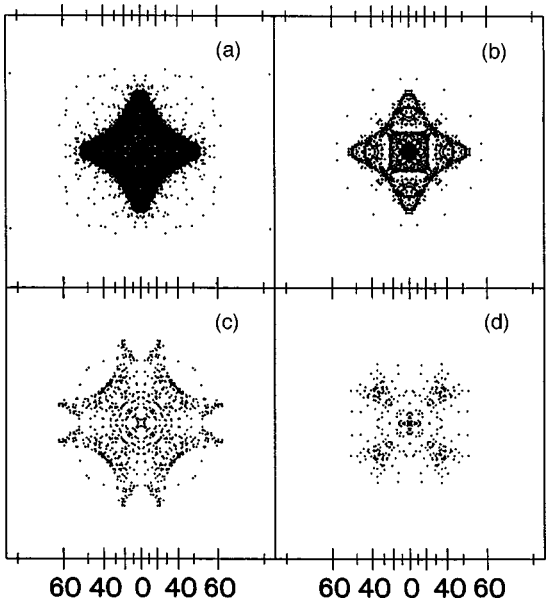

FIG. 2. Calculated spot patterns formed by the ejection of atoms from (a) and (c) the first atomic layer, and (b) and (d) the second layer of the Ag{100} surface due to 2-keV Ar-atom bombardment at a normal incident angle. The kinetic energy of ejection is between 20 and 40 eV for (a) and (b), and between 220 and 240 eV for (c) and (d). The radial distance is the polar angle of ejection in degrees as given by the scale on the abscissa. The intensity factor relative to that of (a) and (b) is 5 for (c) and (d).

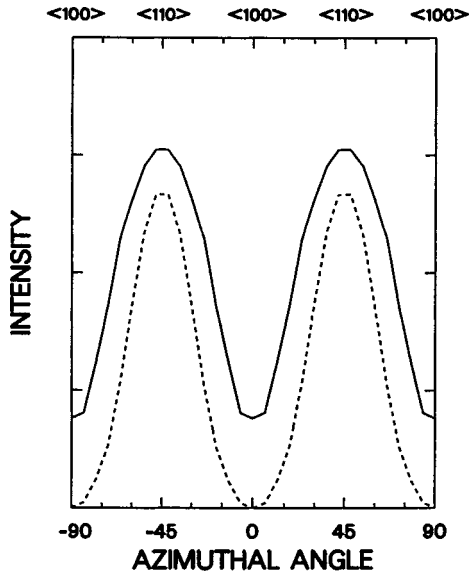

FIG. 3. Calculated dependence on azimuthal angle of Ag atoms sputtered with kinetic energies of between 220 and 240 eV from the first (solid curve) and the second (dashed curve) atomic layers of the Ag{100} surface due to bombardment of 2-keV Ar atoms at a normal incident angle. The polar angle of detection is 45°, and the angular resolution is ±7°.

tively. As expected for atoms sputtered with energies of more than 20 eV,[2(a)] all the patterns in Fig. 2 show relatively intense spot regions with noticeable azimuthal anisotropy. Regardless of the layer from which atom ejection takes place, the spot patterns i.e., Figs. 2(a) and 2(b) formed by the (30±10)-eV atoms reveal a preferential direction of sputtering along the ⟨100⟩ azimuth. The (230±10)-eV atoms ejected from the first layer, on the other hand, form a pattern in which the spots are more scattered. Preferential sputtering along the ⟨100⟩ azimuth is not as distinctively observed in Fig. 2(c) for the (230±10)-eV atoms as in Fig. 2(a) for the (30±10)-eV atoms. Furthermore, the ejection of the (230±10)-eV atoms from the second layer produces an image which has intense spots located in regions very different from that of the image formed by the (30±10)-eV atoms. As shown in Fig. 2(d) the spot density along the ⟨110⟩ azimuth is higher than that along the ⟨100⟩ azimuth, indicating that atoms emitting with energies of 230±10 eV from the second layer are more constrained to proceed along the ⟨110⟩ azimuth. The preferential sputtering along the ⟨110⟩ azimuth of the atoms initially residing in the second layer may thus contribute significantly to the anomalous angular distribution observed in Fig. 1 in the high-energy range of 230±10 eV.

However, unless the sputter yield of the atoms from the second layer constitutes a significant portion of the total yield, the angular distribution of the sputtered particles from the surface may then be mainly determined by the sputtering behavior of the first-layer atoms. The layered contribution to the sputter yield measured along various directions is thus studied to assess the significance of the preferential sputtering along the ⟨110⟩ azimuth of the second-layer atoms to the angular distribution observed in Fig. 1. In Fig. 3, the yields, at a polar angle of 45°, of the atoms sputtered from different atomic layers are shown for atoms ejecting with energies of 230±10 eV. Atoms sputtered from the second layer are found to contribute about 45% of the peak intensity at ⟨110⟩. No atoms with energies of 230±10 eV are found to be ejected from the third layer or below of the Ag{100} surface. Since a significant portion of the sputter intensity at ⟨110⟩ is from the ejection of the atoms from the second layer, the preferential sputtering of the second-layer atoms should thus play an important role in determining the angular distribution of the sputtered particles with high kinetic energies.

The layered contribution to the angular anisotropy in the azimuthal distribution of sputtered particles is then investigated for atoms sputtered with high kinetic energies. Angular anisotropy of the sputtered particles affects the accuracy and easiness in utilizing secondary particle mass spectrometry for structural determination of surfaces.[11–14] The degree of azimuthal anisotropy may be evaluated by taking the ratio of the minimum to the maximum sputter intensity in the angular distribution as the isotropy value. The smaller the value, the larger the angular anisotropy. The value equals 1 if the angular distribution is isotropic. Based on the distribution shown in Fig. 3, the isotropy value for the (230±10)-eV atoms is found to be about zero for atoms sputtered from the second atomic layer of the surface, whereas for those sputtered from the first layer the value is 0.27. The anisotropic sputtering of the atoms from the second layer is thus the major source of the angular anisotropy exhibited in the azimuthal angle distribution of the (230±10)-eV atoms, shown in Fig. 1.

For comparison, the layered contribution to the total sputter yield of atoms ejecting with energies of 30±10 eV is also studied. The result shows that the isotropy value for the (30±10)-eV atoms sputtered from the first atomic layer is as low as 0.19, with the preferential direction of ejection located along the ⟨100⟩ azimuth. In addition, similar to what was found in previous studies on fcc{100},[30,31] the majority

(about 88%) of the atoms sputtered with kinetic energies of 30 ± 10 eV is from the first layer. Atoms ejecting from the third layer or below mainly contribute to the sputter intensity at the ⟨110⟩ azimuth instead. Comparing the layered contributions to the total sputter yields of atoms ejecting with different energies indicates that the angular distribution of the 30 ± 10-eV atoms is dominated by the anisotropic sputtering of atoms from the first layer which has a directional preference along the ⟨100⟩ azimuth, whereas the distribution of the (230 ± 10)-eV atoms is decided by the anisotropic sputtering of atoms from both the first and second layers, which has a directional preference along the ⟨110⟩ azimuth.

In order to understand further the detail of the collision processes which lead to the ejection of high-energy atoms along the ⟨110⟩ azimuth, atomic movement of the surface atom during sputtering is then examined. Understanding the fundamental mechanisms responsible for the sputtering process allows us to relate the observable quantities to their microscopic causes, as well as to predict surface properties from the experimental measurements.[17,31–35] The mechanistic information is usually obtained by physically tracing individual cascades which result in particles sputtered with some particular properties of interest from the surface. In order to extract, from a large number of cascades, the collision sequences which are statistically important, various graphical representations of the cascade have been developed.[20,36–40] Among them, time-exposure cascade analysis[20] is employed in this study. This analysis allows a visualization of the entire collision cascade initiated by the primary particle. With this analytical approach, important collision events involved in each cascade can be quickly evaluated, and the analysis on the evolution of the cascade in space and time can be done in great detail. The disadvantage of this approach, however, is that the key collision sequence may not be able to be mechanistically deconvoluted if the incident energy is dissipated on the surface over a long period of time, and a complex cascade is developed locally in a small region of the surface. Since the high-energy particles take off from the surface shortly after the primary impact and the associated cascades are not complex, time-exposure cascade analysis is particularly useful in studying the mechanistic detail of the high-energy sputtering events.

Our time-exposure cascade analyses of the high-energy sputtering events indicate that there are five major ejection processes which contribute to the maximum sputter intensity along the ⟨110⟩ azimuth for atoms sputtered with energies of 230 ± 10 eV. Three of them are related to a mechanism with which a surface atom is ejected because of its direct collision by the primary particle. An example of this mechanism is shown in Fig. 4. In this figure, a time-integrated atomic motion of the surface after particle bombardment is depicted by using circles of different shades to represent the surface atoms in different atomic layers. The open circles represent the first-layer surface atoms, and the dotted circles represent the atoms in the second layer. The size of the atom indicates the vertical displacement of the atom, with the larger size representing the atom that is closer to the observer. The thickness of the circle is used to show the time interval after the primary impact, with the thinner circles representing the atomic motion occurring in the earlier stage of the collision cascade. Furthermore, a series of symbols is used to show the motion

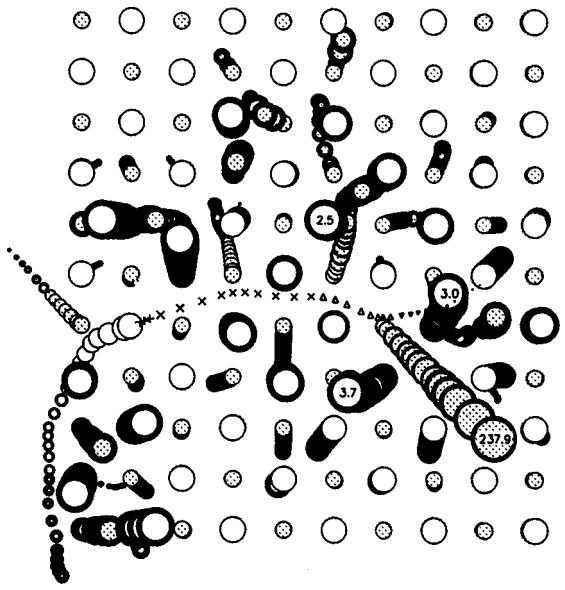

FIG. 4. Time-exposure collision cascade induced in the Ag{100} surface by bombardment of 2-keV Ar atoms at normal incidence. The surface is shown here as viewed from the top. Only the atomic movement close to the point of the primary impact in the top two atomic layers of the surface is shown.

of the primary particle, with the plus (+) representing the particle motion above the first atomic layer of the surface, the cross (×) the motion between the first and second atomic layers, the upright triangle (△) the motion between the second and third layers, and the inverted triangle (▽) the motion between the third and fourth layers. The primary particle thus hits the crystal surface at the point where a change of the symbol from the plus to the cross is observed.

Figure 4 shows the ejection of a high-energy surface atom along the ⟨110⟩ azimuth due to a direct collision by the primary particle after the particle travels in the space between two adjacent {100} atomic planes perpendicular to the surface. As shown in Fig. 4, the incidence of the energetic primary particle causes the target atom at the middle left-hand side of this figure to move into the bulk rapidly. The primary particle then travels downward in the space between two {100} planes perpendicular to the surface, before it strikes a second-layer atom from underneath. The atom struck is thus pushed up and ejects from the surface along the ⟨110⟩ azimuth, with a kinetic energy of 237.9 eV.

The ejection mechanism shown in Fig. 4 can be sketched in a simplified fashion, as presented in Fig. 5(a), in which only two adjacent {100} atomic planes perpendicular to the surface are shown. These two planes define the moving space of the primary particle in the surface. Further cascade analyses show that the primary particle may travel 1–3 lattice spacings between these two perpendicular {100} planes before driving either a first- or a second-layer atom to move up above the surface with a large kinetic energy of ejection along the ⟨110⟩ azimuth.

Other major ejection processes associated with the direct collision of the surface atom by the primary particle are shown in Figs. 5(b) and 5(c) for atoms emitting along the ⟨110⟩ azimuth with kinetic energies of 230 ± 10 eV. As shown in Fig. 5(b), the energetic primary atom may move downward in the {110} plane perpendicular to the surface

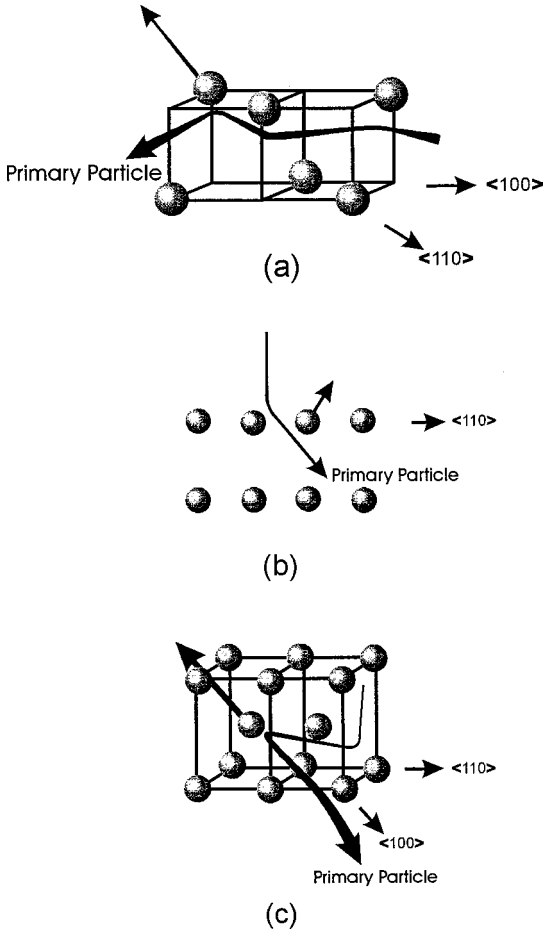

FIG. 5. Schematic diagrams showing the preferred mechanisms of ejection of surface atoms due to a direct collision of the primary atom after it (a) travels in the space between two perpendicular {100} atomic planes, (b) is deflected by the larget atom to move down in the {110} atomic plane perpendicular to the surface, and (c) is scattered by a lower-layer surface atom to proceed upward in the perpendicular {110} plane to behind a higher-layer atom. The thicker the path of the incident trajectory, the more the primary atom is moving toward the viewer.

and cause a surface atom, which is one of the nearest neighbors of the target atom, to eject with a large kinetic energy along the ⟨110⟩ azimuth. In addition to the ejection of the first-layer surface atom, a second-layer atom may also be sputtered through this process when the target atom is located in the second atomic layer. Figure 5(c) shows that the surface atom may also be struck out of the surface with a high ejection energy along the ⟨110⟩ azimuth by a head-on collision with the primary particle from underneath the atom after the particle is backscattered from deeper surface layers.

The other two of the five major processes which result in the high-energy ejection along the ⟨110⟩ azimuth are associated with a mechanism through which an atom is knocked out of the surface by another fast-moving surface atom. The fast-moving atom is generated by a direct collision from the primary particle. The ejection takes place either due to a head-on collision from underneath or to a collision by the fast-moving atom traveling in the space between two {100} atomic planes perpendicular to the surface. Presented in Fig. 6 is an example of the latter case. As shown in the figure, the

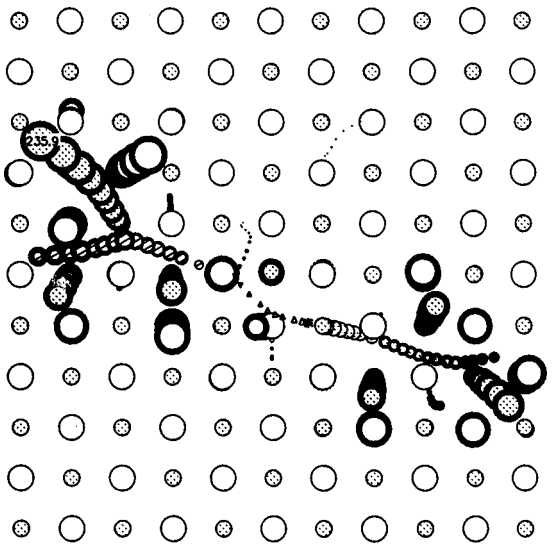

FIG. 6. Time-exposure collision cascade induced in the Ag{100} surface by bombardment of 2-keV Ar atoms at normal incidence. Only the atomic movement close to the point of the primary impact in the top three atomic layers of the surface is shown.

primary particle penetrates quickly into the bulk following its collision on the target atom. During the penetration, it forces a third-layer atom, represented by the hatched circle, to travel fast in the space between two perpendicular {100} planes. The third-layer atom in turn strikes a second-layer atom out of the surface with a kinetic energy of 235.9 eV.

Ejection processes similar to the one shown in Fig. 6 may also take place for a first-layer atom to be knocked out of the surface, with a high ejection energy along the ⟨110⟩ azimuth, by an energetic second-layer atom traveling in the space between two perpendicular {100} planes. In some cases, the second-layer atom may itself also emit with a high kinetic energy along another ⟨110⟩ direction which is 90° away from the azimuth of ejection of the first-layer atom. We note that no high-energy ejection along the ⟨110⟩ azimuth is found to take place for atoms knocked out of the surface by their adjacent atoms in the same atomic layer.

Presented in Fig. 7 is an example of the high-energy atoms sputtered along the ⟨110⟩ azimuth due to a head-on collision by a fast-moving atom from underneath. As shown in this figure, the primary particle is scattered by a third-layer atom after its collision with the target atom. The scattering is manifested in the figure by a change in the direction of the trajectory of the primary particle. The role of the third-layer atom in causing the primary particle to scatter is revealed by the change of the symbol from an upright triangle to an inverted triangle, indicating that the primary particle is traveling from the space between the second and third atomic layers to that between the third and fourth layers. After the scattering, the primary particle proceeds to cause a third-layer atom to travel upward, which in turn makes a head-on collision with a first-layer atom. This atom in the first layer then ejects from the surface with a kinetic energy of 238.8 eV along the ⟨110⟩ azimuth.

A first-layer particle may also be struck out of the surface by a head-on collision from a second-layer atom. In that case, the collision takes place after the second-layer atom is channeled to move along the space between two ⟨110⟩ rows

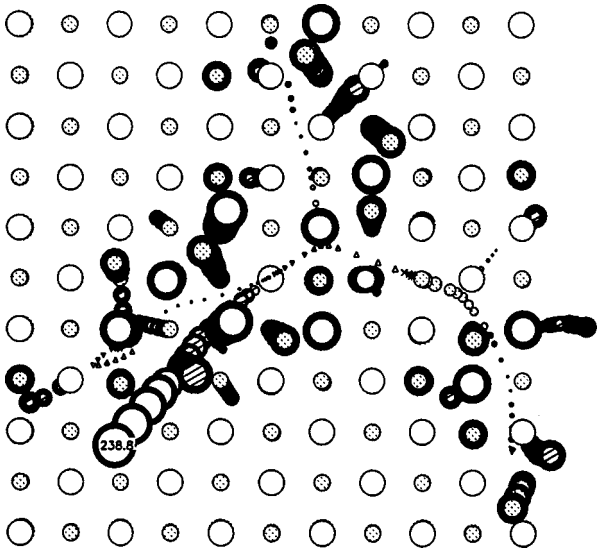

FIG. 7. Time-exposure collision cascade induced in the Ag{100} surface by bombardment of 2-keV Ar atoms at normal incidence. Only the atomic movement close to the point of the primary impact in the top three atomic layers of the surface is shown.

of the second-layer atoms and directly under a ⟨110⟩ row of the first-layer atoms. We note that, although most of the high-energy ejection of atoms initiated by a direct collision from the primary particle takes place at a distance within 2–3 lattice spacings from the point of the primary impact, the two ejection processes initiated by the collision from the fast-moving surface atom may result in a high-energy ejection at a distance of more than three lattice spacings. No atom with a kinetic energy of 230 ± 10 eV is found to be knocked out of the surface through successive head-on collisions, such as what Silsbee proposed[41] in explaining the sputtering of atoms with low energies along the close-packed directions of the crystal lattice. The successive head-on collision process is one of the major mechanisms that cause surface atoms of low kinetic energies to eject along the ⟨211⟩ azimuth from the Ag{111} surface.[20]

The sputtering behavior of all high-energy atoms of more than 150 eV is then studied. Figure 8(a) shows the spot pattern of the atoms ejecting with kinetic energies of more than 150 eV from below the top surface layer. Other than being channeled perpendicularly out of the surface to form the center spot, these high-energy atoms are mostly sputtered along the ⟨110⟩ azimuth. The contribution of the atoms sputtered from each atomic layer with kinetic energies of more than 150 eV to their azimuthal angle distribution obtained at the polar angle of 45° is presented in Fig. 8(b) shown in the figure, very few atoms with ejection energies of more than 150 eV are found to emit along the ⟨100⟩ azimuth from below the first atomic layer to the polar angle of 45°. The ejection of the high-energy atoms from the second layer again plays an important role in deciding the peak position in their azimuthal angle distribution. It shows that atoms ejecting from the second layer contribute about 45% of the peak intensity at the ⟨110⟩ azimuth. The isotropy value for the second-layer atom ejection is about 0.05, whereas the value for ejection from the first layer is 0.52.

Figure 9 shows the comparison of the polar angle distributions along the ⟨110⟩ azimuth with those along the ⟨100⟩

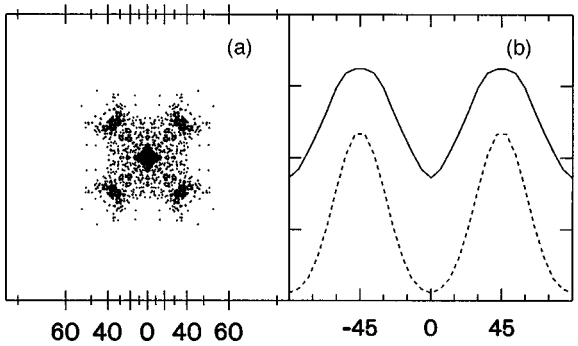

FIG. 8. Calculated angular distribution of atoms with kinetic energies of more than 150 eV sputtered from the Ag{100} surface due to 2-keV Ar atom bombardment at a normal incident angle. (a) is the pot pattern formed by the ejection of atoms from the second layer and below of the surface, and (b) is the calculated dependence on azimuthal angle of the atoms sputtered with the polar angle of $45°\pm7°$ from the first (solid curve) and the second (dashed curve) atomic layers of the surface. The radial distance in (a) is the polar angle of ejection in degrees as given by the scale on the bottom.

azimuth for all the high-energy atoms of more than 150 eV ejecting from different atomic layers. As shown in the figure, the sputter intensity along the ⟨110⟩ azimuth from each layer varies more drastically with the polar angle of ejection than that along the ⟨100⟩ azimuth. More importantly, the sputter intensity from each layer is in general higher along the ⟨110⟩ azimuth than along the ⟨100⟩ azimuth for these high-energy atoms. Figure 9(b) shows that for the entire polar angle distribution along the ⟨110⟩ azimuth, there is a significant contribution of the high-energy atoms ejecting from the second atomic layer to the sputter intensity. In the distribution obtained along the ⟨100⟩ azimuth, as shown in Fig. 9(a), the sputter intensity of the high-energy atoms ejecting at polar angles of greater than ~40° is, however, solely due to the sputtering of the first-layer atoms. Furthermore, the layered

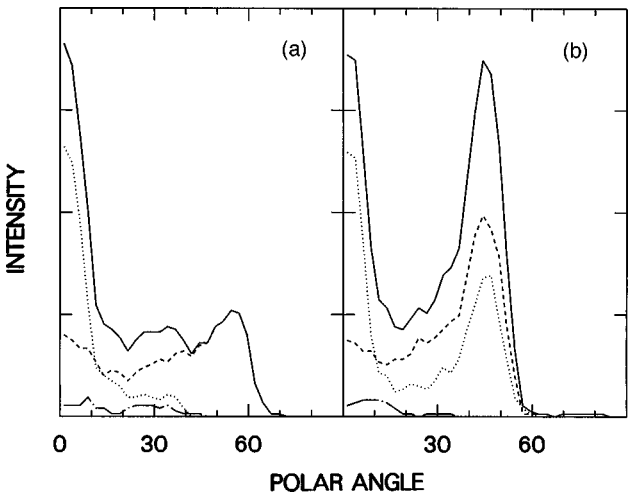

FIG. 9. Calculated dependence on the polar angle of ejection of Ag atoms sputtered with kinetic energies of more than 150 eV along (a) the ⟨100⟩ azimuth, and (b) the ⟨110⟩ azimuth of the Ag{100} surface due to bombardment of 2-keV Ar atoms at a normal incident angle. The angular resolution is ±7°. The solid curve represents the angular distribution of atoms from all layers, the dashed curve the one from the first layer, the dotted curve the one from the second layer, and the dash-dotted curve the third layer.

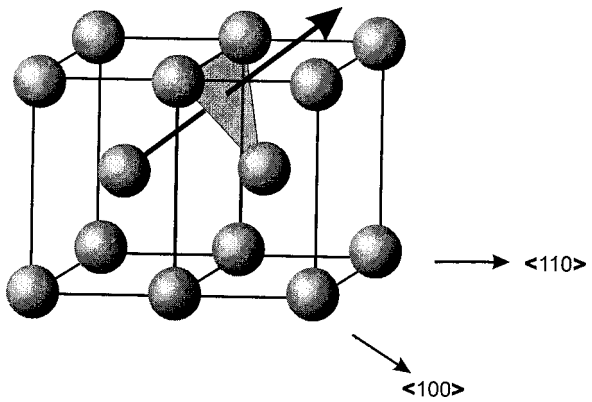

FIG. 10. Schematic diagram showing the ejection pathway of atoms with kinetic energies of more than 150 eV from the second layer of the Ag{100} surface due to 2-keV Ar-atom bombardment at a normal incident angle.

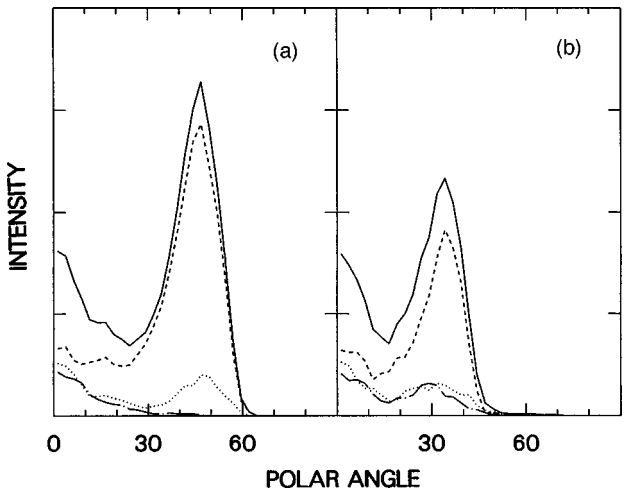

FIG. 11. Calculated dependence on the polar angle of ejection of Ag atoms sputtered with kinetic energies between 20 and 40 eV along (a) the ⟨100⟩ azimuth, and (b) the ⟨110⟩ azimuth of the Ag{100} surface due to bombardment of 2-keV Ar atoms at a normal incident angle. The angular resolution is ±7°. The solid curve represents the angular distribution of atoms from all layers, the dashed curve the one from the first layer, the dotted curve the one from the second layer, and the dash-dotted curve the third layer.

contribution to the sputter intensity at the normal direction indicates that about 75% of the intense center spot in the atom ejection pattern shown in Fig. 8(a) is due to the ejection of the second-layer atoms. The relatively small contribution of the high-energy atoms ejecting from the first atomic layer to the center-spot intensity may be due to the absence of an atomic arrangement which can properly constrain the path of the ejecting first-layer atoms to the polar angle of ~0°. An ejecting second-layer atom, on the other hand, may be focused by its nearest-neighboring atoms in the first layer such that it emits normal to the surface. Figure 9 thus reveals that, in addition to the details of the collision process, the number of the atoms ejecting from below the first layer and the presence of a proper surface atomic arrangement for confining the ejection path may significantly affect the sputtering properties of the high-energy atoms.

The influence of the surface atomic arrangement on the directional preference of sputtering of the high-energy atoms is further studied. It shows in Fig. 9 that along the ⟨110⟩ azimuth the maximum sputter intensity of the high-energy atoms occurs at a polar angle of ~46°, in addition to the one observed at 0°. Examining the lattice model of the fcc{100} crystallite reveals that for sputtering to take place at this polar angle along the ⟨110⟩ azimuth, the high-energy atom ejecting from the second atomic layer will emit through the space of an inverted triangle, as depicted schematically in Fig. 10. This triangle is defined by the three nearest neighbors of the ejecting atom along the sputtering trajectory. Two of these neighbors are located in the upper layer, and one is in the same layer as the one from which the atom ejects. Trajectory analysis of the ejecting atom shows that, although in this case the ejecting atom is very energetic, the repulsive interaction of this atom with those outlining the triangle is able to force this atom to move mostly through this triangular space. The path of the ejecting atom is thus constrained and consequently, the sputter intensity is enhanced at the ⟨110⟩ azimuth.

The sputtering property of the high-energy atoms appears to be quite different from that of the low-energy atoms. Presented in Figs. 11(a) and 11(b) are the polar angle distributions of the atoms sputtered with low kinetic energies of 30±10 eV along the ⟨100⟩ and ⟨110⟩ azimuths, respectively. Comparing Fig. 9 with Fig. 11 shows that the sputter intensity of the (30±10)-eV atoms rises to its maximum at a polar angle considerably smaller than that of the atoms with ejection energies of more than 150 eV. This indicates that the major ejection mechanisms of the low-energy atoms may be very different from those of the high-energy atoms. For example, Fig. 11(b) shows that the maximum intensity of the (30±10)-eV atoms sputtered along the ⟨110⟩ azimuth occurs at a polar angle of ~34° from the surface normal. This peak polar angle is close to the one observed previously[19] for Rh atoms sputtered with energies of 20–50 eV along the ⟨110⟩ azimuth from the Rh{100} surface, which have a maximum sputter intensity at 35°. It reveals that the constraint on the path of the ejecting atoms by the atoms outlining the inverted triangle shown in Fig. 10 may not be a major cause governing the ejection direction of these low-energy atoms, since the face of the triangle is tilted by an angle of more than 45°. Figure 11 also shows that the angular distributions obtained at 30±10 eV along the ⟨100⟩ and ⟨110⟩ azimuths, respectively, are both predominately determined by the atoms sputtered from the first layer. Furthermore, in contrast to what is observed in the distribution of the high-energy atoms, the intensity of the low-energy atoms at a polar angle of 0° is not mainly decided by the atoms sputtered from the lower layers, although, at small polar angles, the low-energy atoms ejecting from the second and third atomic layers have a relatively higher contribution to the sputter intensity than at large polar angles. Figure 11 thus reveals that the focusing process of the ejecting low-energy atoms by the atoms located in the upper layers of the surface does not significantly affect the angular distribution of the low-energy atoms. On the other hand, as discussed above, the focusing of the high-energy atoms ejecting from the lower layers by the atoms in the upper layers is a major process in determining their directions of ejection.

The sputtering of the high-energy atoms may thus be utilized for analyzing the geometric structure of the second

atomic layer relative to that of the first layer. According to the theories proposed by Harrison[42] and Lehman and Sigmund,[43] the ejection direction of sputtered particles is ultimately governed by the geometric structure in the top few atomic layers of the surface. Garrison and Winograd[2] suggested that the appearance of the maximum sputter intensity at the ⟨100⟩ azimuth for the low-energy atoms sputtered from a clean fcc{100} surface is due to the constraint on the ejection path of the first-layer atom by the presence of its two nearest-neighboring atoms, which form an open channel along the ⟨100⟩ azimuth, in the same layer. Our present study shows that by increasing the ejection energy from 30 ± 10 eV to more than 150 eV, the contribution of the atoms sputtered from the second layer to the total sputter yield increases considerably from less than 15% to more than 40%. It is this substantial increase in the relative sputter yield of the second-layer atom which provides, in this case, a signature of the geometry of the second layer. This geometric information may be predicted by extending Garrison and Winograd's argument to the ejection of atoms from the lower layers, i.e., the high-energy atoms ejecting from the second layer tend to be confined to proceed preferentially along an azimuth along which the emitting path of the atoms from the lower layers is least obstructed. In the case of fcc{100}, it is the ⟨110⟩ azimuth along which a high-energy atom can emit because of the presence of a surface semichannel. This surface semichannel is constituted by the first-layer atoms as the wall of the semichannel, and by the second-layer atoms as the base. Tracing individual sputtering trajectories shows that, after being focused by the triangular atomic feature shown in Fig. 10, the high-energy atoms sputtered from the second layer are mostly confined along the semichannels to eject from the surface. The confinement of the ejecting atoms along surface semichannels results in higher sputter intensities at all polar angles along the ⟨110⟩ azimuth than along the ⟨100⟩ azimuth for the high-energy atoms sputtered from the second layer, as observed in Fig. 9. The angular distribution of the low-energy atoms thus mostly reflects the geometric structure of the first atomic layer, whereas the distribution of the high-energy atoms of more than 150 eV reveals the atomic arrangement, such as the orientation of the surface semichannel present, in the upper surface layers, from which the geometry of the second atomic layer can be deduced.

IV. CONCLUSIONS

The peak position in the azimuthal angle distribution of the atoms sputtered from the Ag{100} surface is sensitive to the ejection energy of these atoms. As the ejection energy is increased from tens to hundreds of eV, the peak position shifts from the ⟨100⟩ to ⟨110⟩ azimuth. The occurrence of the maximum sputter intensity at the ⟨110⟩ azimuth in the high-energy range is associated with the details of the major ejection process of the atoms sputtered from the surface, with a substantial increase in the relative sputter yield of the atoms ejecting from below the first layer, and with the presence of unique structural features on the surface. The high-energy atoms may prefer to eject along the ⟨110⟩ azimuth from the surface due to a direction collision by the primary particle or to a strike by another fast-moving surface atom following its energetic traveling in a space between two adjacent {100} atomic planes perpendicular to the surface. The preferential ejection of the high-energy atoms along the ⟨110⟩ azimuth may also be caused by a head-on collision from either the primary particle or a fast-moving surface atom. The atoms ejecting from the second layer with high kinetic energies may be focused to proceed through the space among its three nearest neighbors along the ejecting trajectory, and then confined by a ⟨110⟩ surface semichannel before leaving the surface.

The present study demonstrates that when combined with the computer simulation, the angle-resolved secondary particle mass spectrometry is a valuable tool for characterizing the chemical bonding structures of the surface. The computer simulation can provide, among other things, invaluable insights into the detail of the sputtering process, from which important information about the property of the surface may be extracted. For example, results of this study reveal that by utilizing the sputtering characteristics of the high-energy atoms, the geometric structure of the second atomic layer in the surface may be appropriately described. The preferred ejection direction of the high-energy atoms is along the azimuth where the path of the ejecting atoms from the second layer is least obstructed by the atoms present in the first layer. Information about the cause of the variation in the peak angle of sputtering, due to a change in the detection condition, can also be extracted. This more detailed understanding of the collision-induced process is essential to an exploration of the ultimate capability of the angle-resolved secondary particle mass spectrometry in determining surface structures. It also allows us to understand better the initiation and formation of the ion-induced surface damage,[44] as well as the enhancement of the catalytic activity of the ion-irradiated surface.[45,46]

ACKNOWLEDGMENTS

The financial support of the ROC National Science Council and the Chinese Petroleum Corporation is gratefully acknowledged.

*Author to whom correspondence should be addressed.

[1] See, for example, T. E. Madey and J. T. Yates, Surf. Sci. **63**, 203 (1977); H. Ibach, H. Hopster, and B. Sexton, Appl. Surf. Sci. **1**, 1 (1977); N. Winograd, J. P. Baxter, and F. M. Kimock, Chem. Phys. Lett. **89**, 581 (1982); J. A. Yarmoff, D. M. Cyr, J. H. Huang, S. Kim, and R. S. Williams, Phys. Rev. B **33**, 3856 (1986); C. S. Fadley, Phys. Scr. **T17**, 39 (1987); F. Masson, H. Bu, M. Shi, and J. W. Rabalais, Surf. Sci. **249**, 313 (1991).

[2] (a) N. Winograd, B. J. Garrison, and D. E. Harrison, Jr., Phys. Rev. Lett. **41**, 1120 (1978); (b) S. P. Holland, B. J. Garrison, and N. Winograd, *ibid.* **43**, 220 (1979).

[3] R. A. Gibbs, S. P. Holland, K. E. Foley, B. J. Garrison, and N. Winograd, J. Chem. Phys. **76**, 684 (1982).

[4] P. H. Kobrin, G. A. Schick, J. P. Baxter, and N. Winograd, Rev. Sci. Instrum. **57**, 1354 (1986); N. Winograd, Mat. Fys. Medd. K. Dan. Vidensk. Selsk. **43**, 223 (1993).

[5] C.-C. Chang and N. Winograd, Surf. Sci. **230**, 27 (1990).

[6] (a) S. A. Larson and L. L. Lauderback, Surf. Sci. **284**, 1 (1993);

(b) L. L. Lauderback, A. J. Lynn, C. J. Waltman, and S. A. Larson, *ibid.* **243**, 323 (1991).
[7] C. He, Z. Postawa, M. El-Maazawi, S. Rosencrance, B. J. Garrison, and N. Winograd, J. Chem. Phys. **101**, 6226 (1994).
[8] A. Li and R. O. Watts, J. Chem. Phys. **103**, 7187 (1995).
[9] C. T. Reimann, M. El-Maazawi, K. Walzl, B. J. Garrison, N. Winograd, and D. M. Deaven, J. Chem. Phys. **90**, 2027 (1989).
[10] N. Winograd, *Chemistry and Physics of Solid Surfaces V*, edited by R. Vanselow and R. Howe, Springer Series in Chemical Physics Vol. 35 (Springer, New York, 1983), p. 403.
[11] G. K. Wehner, J. Appl. Phys. **26**, 1056 (1955).
[12] A. L. Southern, W. R. Willis, and M. T. Robinson, J. Appl. Phys. **34**, 153 (1963).
[13] R. S. Nelson and M. W. Thompson, Phys. Lett. **2**, 124 (1962).
[14] T. Nagayama, K. Noguchi, S. Sasaki, and R. Shimizu, Nucl. Instrum. Methods Phys. Res. B **39**, 91 (1989).
[15] D. W. Moon, R. J. Bleiler, and N. Winograd, J. Chem. Phys. **85**, 1097 (1986).
[16] S. Kapur and B. Garrison, J. Chem. Phys. **75**, 445 (1981).
[17] C. T. Reimann, M. El-Maazawi, K. Walzl, B. J. Garrison, N. Winograd, and D. M. Deaven, J. Chem. Phys. **90**, 2027 (1989).
[18] N. Winograd, M. El-Maazawi, R. Maboudian, Z. Postawa, D. N. Bernardo, and B. J. Garrison, J. Chem. Phys. **96**, 6314 (1992).
[19] R. Maboudian, Z. Postawa, M. El-Maazawi, B. J. Garrison, and N. Winograd, Phys. Rev. B **42**, 7311 (1990).
[20] C.-C. Chang, Phys. Rev. B **48**, 12 399 (1993).
[21] D. E. Harrison, Jr., P. W. Kelly, B. J. Garrison, and N. Winograd, Surf. Sci. **76**, 311 (1978).
[22] D. E. Harrison, Jr., Crit. Rev. Solid State Mater. Sci. **14**, S1 (1988).
[23] B. J. Garrison, Chem. Soc. Rev. **21**, 155 (1992).
[24] D. N. Bernardo, R. Bhatia, and B. J. Garrison, Comput. Phys. Commun. **80**, 259 (1994).
[25] G. Moliere, Z. Naturforsch. **2A**, 133 (1947).
[26] O. B. Firsov, Zh. Eksp. Teor. Fiz. **33**, 696 (1957) [Sov. Phys. JETP **6**, 534 (1958)].
[27] D. J. O'Connor and J. P. Biersack, Nucl. Instrum. Methods Phys. Res. B **15**, 14 (1986).
[28] C.-C. Chang, Surf. Interface Anal. **15**, 79 (1990).
[29] C.-C. Chang, N. Winograd, and B. J. Garrison, Surf. Sci. **202**, 309 (1988).
[30] D. E. Harrison, Jr., P. W. Kelly, B. J. Garrison, and N. Winograd, Surf. Sci. **76**, 311 (1978).
[31] S. W. Rosencrance, J. S. Burnham, D. E. Sanders, C. He, B. J. Garrison, N. Winograd, Z. Postawa, and A. E. DePristo, Phys. Rev. B **52**, 6006 (1995).
[32] C.-C. Chang, H. H. Chen, and P. Wu, in *Microstructure of Irradiated Materials*, edited by I. M. Robertson, S. J. Zinke, L. E. Rehn, and W. J. Phythian, MRS Symposia Proceedings No. 373 (Materials Research Society, Pittsburgh, 1995), p. 35.
[33] M. Hou and W. Eckstein, Nucl. Instrum. Methods Phys. Res. B **13**, 324 (1986).
[34] M. Hou and W. Eckstein, Phys. Rev. B **42**, 5959 (1990).
[35] R. Bhatia and B. J. Garrison, J. Chem. Phys. **100**, 8437 (1994).
[36] S. P. Holland, B. J. Garrison, and N. Winograd, Phys. Rev. Lett. **43**, 220 (1979); **44**, 756 (1980).
[37] R. P. Webb and D. E. Harrison, Jr., Nucl. Instrum. Methods Phys. Res. B **218**, 727 (1983).
[38] N. Winograd, B. J. Garrison, and D. E. Harrison, Jr., J. Chem. Phys. **73**, 3473 (1980).
[39] M. H. Shapiro and T. A. Tombrello, Nucl. Instrum. Methods Phys. Res. B **84**, 453 (1994).
[40] D. E. Sanders, K. B. S. Prasad, J. S. Burnham, and B. J. Garrison, Phys. Rev. B **50**, 5358 (1994).
[41] R. H. Silsbee, J. Appl. Phys. **28**, 1246 (1957).
[42] D. E. Harrison, J. P. Johnson, and N. S. Levy, Appl. Phys. Lett. **8**, 33 (1966).
[43] C. Lehman and P. Sigmund, Phys. Status Solidi **16**, 507 (1966).
[44] A. H. Al-Bayati, K. G. Orrman-Rossiter, and D. G. Armour, Surf. Sci. **249**, 293 (1991).
[45] A. Berko and H. P. Bonzel, Surf. Sci. **251/252**, 1112 (1991).
[46] Jiun-Chan Yang, M.S. thesis, National Taiwan University, 1997.